J Appl Electrochem (2011) 41:731–740
DOI 10.1007/s10800-011-0289-9

ORIGINAL PAPER

Cathodic behaviour of $CoFe_2O_4$ spinel electrodes in alkaline medium

E. Laouini · J. Douch · M. Hamdani · Y. Berghoute · M. H. Mendonça · M. I. S. Pereira · R. N. Singh

Received: 15 November 2010 / Accepted: 13 March 2011 / Published online: 3 April 2011

Abstract Spinel type $CoFe_2O_4$ thin films have been prepared, on stainless steel supports, by thermal decomposition of aqueous solutions of mixed cobalt and iron nitrates in 1:2 molar ratio at 400 °C. The electrochemical behaviour of the $CoFe_2O_4$/1 M KOH interface was investigated by cyclic voltammetry, chronoamperometry and impedance techniques. The studies allowed finding out the redox reactions occurring at the oxide surface. The results were compared with colloidal electrodes prepared by alkaline precipitation of Fe(II) or Fe(III) hydrous oxihydroxides on platinum electrodes. In addition, it has been concluded that the processes are diffusion-controlled and the diffusion of the hydroxide ion, through the oxide, acts as the rate-determining step. The diffusion coefficient of OH^- through the oxide film was determined using cyclic voltammetry, chronoamperometry and electrochemical impedance spectroscopy techniques.

Keywords Mixed oxide films · Cobalt iron oxide electrode · Iron hydroxide electrodes · Cyclic voltammetry · Oxygen reduction

E. Laouini · J. Douch · M. Hamdani (✉) · Y. Berghoute
Laboratoire de Chimie Physique, Faculté des Sciences, Université Ibn Zohr, B.P. 8106 Cité Dakhla, Agadir, Morocco
e-mail: hamdani.mohamed@gmail.com

M. H. Mendonça · M. I. S. Pereira
Centro de Ciências Moleculares e Materiais, Faculdade de Ciências da Universidade de Lisboa, Lisbon, Portugal
e-mail: misp@fc.ul.pt

R. N. Singh
Department of Chemistry, Faculty of Science, Banaras Hindu University, Varanasi 221 005, India
e-mail: rnsbhu@rediffmail.com

1 Introduction

Fe–Co mixed metallic oxides have received considerable attention due to their wide availability, low cost and several applications in modern information technology [1]. Among Fe–Co oxides, the spinel cobalt ferrite oxide, $CoFe_2O_4$, presents interesting electrochemical properties and a good stability in alkaline solutions. Recently, cobalt ferrite oxide electrodes were studied as anodes for batteries [2–4] and the oxygen evolution reaction (OER) [5]. On the other hand, polypyrrole/$CoFe_2O_4$ composite films have been studied as cathode for the oxygen reduction reaction (ORR) [6].

It is well known that the preparation method has a strong influence on the oxide's physicochemical and electrocatalytic properties. Different methods, such as electrochemical deposition [7, 8], thermal decomposition [9], precipitation [5, 6, 10], sol–gel [3, 11, 12], and spray pyrolysis [13], have been used to prepare $CoFe_2O_4$. Recently, $CoFe_2O_4$ nanoparticles were prepared by co-precipitation of ferric and cobaltous ions with sodium hydroxide [14] and also by spraying co-precipitation [15].

The redox transitions taking place on these oxide electrodes play a crucial role on their electrocatalytic activities and its study is very important in view of potential application as electrocatalyst. Indeed, these studies are scanty despite their use as electrode materials. There are few articles dealing with the electrochemical behaviour of $CoFe_2O_4$ oxides. Godinho et al. [16] studied the effect of the partial replacement of Fe by Ni and/or Mn on the electrocatalytic activity of the Fe/$CoFe_2O_4$ thin film oxide electrode for the OER. The same group studied, also, the solid-state surface redox transitions on $FeCo_2O_4$ pelleted electrode [10]. On the other hand, with the aim to improve its electrocatalytic activity towards the OER, the influence

of the partial substitution of Fe by Cr in the $CoFe_2O_4$ was also investigated [5]. Moreover, some more information is given in our recent study dealing with the electrochemical behaviour of $Co_xFe_{3-x}O_4$ ($x = 0$, 1, 2 and 3) [17], where it is shown that $CoFe_2O_4$ electrodes, under cycling conditions, behave like Fe_3O_4 and Co_3O_4 oxides on the cathodic and anodic potential ranges, respectively.

The application of electrochemical impedance spectroscopy (EIS) to characterize the electrochemical and electrocatalytic interfacial properties has been used, recently, in the study of the oxygen reaction in alkaline solutions. Such an oxide catalyst/electrolyte interface can be represented by a simple equivalent circuit model: $LR_s(R_1Q_1)$ (R_2Q_2) (R_3Q_3), where (R_1Q_1), (R_2Q_2), and (R_3Q_3) correspond to the capacitive and resistive contributions of the catalyst layer/support interface, the bulk catalyst mass, and the electrolyte/catalyst surface, respectively and R_s and L are the solution resistance and inductance, respectively. L includes the contribution from the cell connections and their interaction with the surroundings, if any, at high frequencies [18]. An equivalent circuit, $LR_s(R_1Q_1)$ (R_2Q_2) has been employed by Laouini et al. [19–21] to simulate the experimental data and estimate the circuit parameters, of Fe–Co_3O_4 films (0, 5, and 10% Fe) in 1 M KOH at different positive potentials.

Silva et al. [22] characterized cobalt oxide coatings on cold rolled steel in alkaline sodium sulphate solution by EIS. The experimental data best fit was obtained with the equivalent circuit, R_s $(R_{ct}Q_{dl})$ (R_fQ_f), where R_s, R_{ct}, and R_f and Q_f and Q_{dl} correspond to the solution, charge transfer and oxide film resistances and the constant phase elements (CPE) for the film and double layer, respectively.

Wu et al. [23] studied the OER on the Co + Ni mixed oxide electrodeposited films on Ni in 1 M NaOH at 25 °C by EIS. The equivalent circuit, $R_s(C_{dl}(R_{ct}(C_pR_p)))$, was used to model the impedance response and estimate the circuit parameters. C_{dl}, R_{ct}, C_p and R_p are the double layer capacitance, charge transfer resistance, pseudo-capacitance and pseudo-resistance, respectively. C_p and R_p are associated with the potential dependent surface coverage of an adsorbed intermediate in the OER mechanism. A similar equivalent circuit, $R_s(C_{dl}(R_{ct}(C_aR_a)))$, was used by Palmas et al. [24] to model Teflon bonded Co_3O_4/Ti and Nafion bonded Co_3O_4/Ti interfaces in 1 M NaOH in the OER region ($E = 0.6$ V vs. SCE). R_aC_a is a parallel element to take into account the possible adsorption of reaction intermediates. Recently, Singh et al. [25] studied Co_3O_4 and La doped Co_3O_4, in the form of thin films on Ni, in 1 M KOH. They used the equivalent circuit $LR_s(R_1Q_1)$ (R_2Q_2) to treat the impedance data. Palmas et al. [26] investigated the Co_3O_4/Ti electrodes behaviour in alkaline solution, during oxidation at different anodic potentials starting from the open circuit potential (E_{OC}) to a potential in the OER region (0–0.6 V vs. SCE) by cyclic voltammetry (CV) vis-a-vis impedance spectroscopy. The impedance study was performed to better characterize the surface solid state redox transitions (SSSRTs). The data were simulated considering the equivalent circuit model, $R_s(R_1Q_1)$ (R_2Q_2), where R_1 and R_2 and Q_1 and Q_2 represent resistances and pseudo capacitances associated with SSSRTs. Studies on the behaviour of the $Cu_xCo_{3-x}O_4$ ($0 \geq x \geq 1$) films, on Ni, by CV and EIS have been presented by Lal et al. [27]. The results show that the variation of C_{dl} as a function of the applied potential (from −0.15 to +0.65 V vs. Hg/HgO), obtained by EIS, is quite similar to the anodic part of the CV curve recorded in the same potential region. They also determined [28] the electrochemical active surface area (EASA) for the spinel type $M_xCo_{3-x}O_4$ (M = Mn, Ni or Cu; $0.25 \geq x \geq 1$) oxide films on Ni in 1 M KOH by CV and EIS in the double layer region. Values obtained by both methods, for a particular oxide composition, were practically the same.

Ho et al. [29] have shown that the Nyquist plot for the modified Randles's circuit presents two distinct diffusion regimes, particularly in the case of porous thin films. The angular frequency (ω) range, over which these regimes are observed, depends on the product, kL, where L is the film thickness, $k = (\omega/2D_{ap})^{1/2}$ and D_a is the apparent diffusion coefficient. When $kL \gg 1$, the diffusion layer created by the perturbation is much thinner than the film and a conventional semi-infinite Warburg response ($\Theta = 45°$) is observed. When $kL \ll 1$, the diffusion layer encompasses the entire film. In this case, a finite Warburg response (characterized by $\Theta = 90°$) is observed. D_{ap} can be obtained from both the semi-infinite and finite Warburg regions. In the semi-infinite Warburg region, the magnitude of the impedance ($|Z|$) varies linearly with $(\omega)^{-1/2}$ [30] in the following manner:

$$|Z| = L/C\left(D_{ap}\omega\right)^{1/2} \tag{1}$$

where C is the limiting capacitance. As already reported [30, 31], C is invariant with frequency in the finite diffusion region and is given by:

$$-Z'' = 1/\omega C \tag{2}$$

being Z'' the imaginary component of the impedance.

In this study, the redox transitions, occurring on $CoFe_2O_4$ in alkaline media, are studied in the oxygen reduction potential range by cyclic voltammetry and impedance spectroscopy technique. The results are compared to those obtained on Fe(II) or Fe(III)-hydroxide deposited on Pt substrates. A model of oxide/solution interface, by a suitable electrical equivalent circuit, is presented and the values of the circuit parameters, such as the charge transfer resistance and the double layer capacitance, at different negative potentials in 1 M KOH are estimated.

The OH^- diffusion coefficient through the oxide film was determined using CV, chronoamperometry and EIS methods.

2 Experimental part

2.1 Oxide film preparation

Oxide thin films of cobalt ferrite were prepared by thermal-decomposition of aqueous solution containing nitrates of cobalt and iron in a molar ratio (Co/Fe) of 1:2 as described elsewhere [17]. Scratched stainless steel plates with dimensions of 1 cm × 2 cm × 0.1 cm, were used as substrates for the oxide films preparation. Before use, the steel plates were thoroughly washed with distilled water, ultrasonically cleaned in distilled water and absolute ethanol, for 10 min, and then dried in air. The pre-treatment of the steel surface, prior to coating, is important for the film adherence. The pretreated steel plates were placed in a drying oven at 60 °C and small drops of the mixed metal nitrates solution were dripped on the surface using a syringe. When the steel surface became dry, again, small drops of the solution were dripped on the surface and dried. This procedure was repeated 4–5 times to cover uniformly the entire substrate surface. Finally, the coated steel plates were annealed at 400 °C for 2 h in a tube furnace in air. Following this procedure, black coloured and adherent thin oxide films, with loadings ranging between 2.0 and 2.4 mg cm^{-2} and 0.3–0.4 μm thickness, were obtained. The films present a good adherence to the substrate and were used as prepared.

2.2 Hydroxide films preparation

Fe-hydroxide films were prepared by alkaline precipitation on a Pt rotating disc electrode. Before the deposition, the Pt support with diameter $\phi = 2$ mm, was degreased with absolute ethanol and ultrasonically cleaned in distilled water for 5 min. The hydroxide films were obtained by consecutive immersion of Pt in 0.025 M $FeSO_4$ (or 0.025 M $FeCl_3$) and in 0.1 M KOH solutions. Each immersion takes 10 s at room temperature. The resulting colloidal suspension is then dried in the oven at 90 °C for about 30 min. This procedure was repeated 3–4 times to cover uniformly the substrate surface. The obtained hydroxides using $FeSO_4$ and $FeCl_3$ presented a blue and an orange rusted colour, respectively. These two hydrous oxi-hydroxides are referred to as Fe(II)- and Fe(III)-hydroxides.

2.3 X-ray analysis

The phase purity of the $CoFe_2O_4$-deposited films was studied using X-ray diffraction (XRD) patterns recorded on a Philips PW 1730 diffractometer, equipped with a graphite monochromator coupled to a vertical goniometer PW 1820. The X-ray source Cu–K_α radiation ($\lambda_{k\alpha} = 1.54056$ Å) was operated at 30 mA and 40 kV, with an automatic data acquisition (APD Philips v 3.5B software) facility. The diffractograms were recorded between $2\theta = 15°$ and 80° at a scan rate of 0.02° s^{-1}.The lattice parameters were calculated using the least square refinement technique.

2.4 Electrochemical analysis

2.4.1 Oxide and hydroxide film electrodes

Electrochemical studies were carried out in a conventional three-electrode single compartment glass cell. The potential of the working electrode was measured against a saturated calomel electrode (SCE). The SCE (0.240 V vs. SHE) was connected through a KCl agar–agar salt bridge, the tip of which was placed as close as possible to the surface of the working electrode in order to minimize the solution resistance between the test and reference electrodes. The counter electrode was a platinum plate of 8 cm^2.

The electrical contact with the oxide electrode was made using a crocodile clip on a small strip of the steel plate, oxide free. The back of the electrode was isolated with an inert non-conductive varnish and only a single face, with 2 cm^2, was exposed to the electrolyte.

Electrochemical measurements were made in 1 M KOH at 25 °C. The electrolyte volume was 50 mL and before use was deaerated with N_2 for 20 min. For all the tested electrodes, the open-circuit potential was measured before starting the electrochemical studies.

2.4.2 Techniques and instrumentation

In situ surface, characterization and monitoring of the electrodes were done by cyclic voltammetry, at a sweep rate of 10 mV s^{-1}, or otherwise stated. The electrochemical measurements were carried out using a Voltalab PRZ 100 Radiometer-Analytical apparatus with the VoltaMaster software.

The EIS study was performed using an electrochemical set Voltalab PRZ 100 Radiometer-Analytical and Zview software was used to analyse the data. The experimental impedance data were fitted to an appropriate equivalent circuit using ZsimpWin software. The experimental procedures and conditions employed in the EIS study were similar to those described previously [17].

3 Results and discussion

3.1 X-ray diffraction

The diffractogram of the as deposited $CoFe_2O_4$ film, on the stainless steel substrate, is given in Fig. 1, where a XRD pattern of the stainless steel substrate is also presented. This figure shows that the thermal decomposition of metallic nitrates leads to a crystalline spinel phase. Extra peaks (◇) corresponding to the stainless steel substrate also appear on the $CoFe_2O_4$ pattern. The X-ray diffractogram presents the (311) crystal plane as the most intense. The crystallite followed the face-centred cubic crystal geometry. The unit cell dimension, a_0, of the $CoFe_2O_4$ oxide coatings was found to be 8.385 Å, this value is close to 8.392 Å reported (JCPDS: 22-1086) for the same oxide.

The crystallite size (S) was estimated using the Scherrer's formula [32]:

$$S = k\lambda(\beta \cos\theta)^{-1} \quad (3)$$

where k is the crystallite shape factor which was taken equal to 0.9, λ the wavelength of the radiation source (Cu–K_α with $\lambda = 1.54056$ Å), β the full width at half maximum of the most intense spinel peak in radians and θ the corresponding Bragg reflexion angle in deg. The value of the mean crystallite size calculated from the most intense reflection peak (311) crystal plane is 313 ± 20 Å. Wang et al. [33], using the same method, have estimated the crystallite size of $CoFe_2O_4$ prepared by co-precipitation of Fe^{+2}, Fe^{+3} and Co^{+3} with different Fe^{+2}/Fe^{+3} ratio, using 5 M NaOH, at 60 °C. They have found a decrease of the crystallite size, from 1400 to 200 Å, with the increase of Fe^{+3} content.

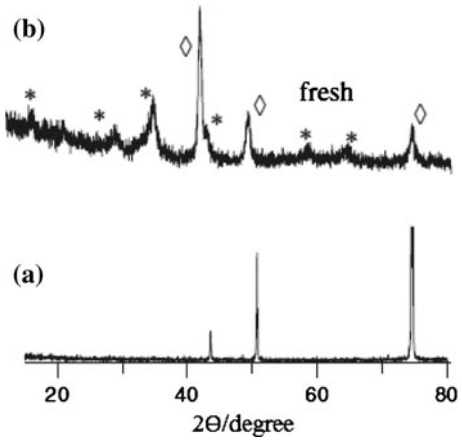

Fig. 1 X-ray diffraction patterns of **a** stainless steel substrate, **b** $CoFe_2O_4$ films prepared by thermal decomposition at 400 °C on a stainless steel substrate, fresh. Marked peaks correspond to the substrate (*diamond*) and to the spinel phase (*asterisk*)

3.2 Electrochemical studies

3.2.1 Cyclic voltammetry

3.2.1.1 $CoFe_2O_4$ oxide electrodes The open-circuit potential, of the $CoFe_2O_4$ oxide electrode in deaerated 1 M KOH solution was found to be around −0.120 V vs. SCE. The time needed to attain a stable value was about 2 min. Figure 2 shows cyclic voltammograms for the $CoFe_2O_4$ electrode, recorded in the potential range of −1.300 to 0.500 V vs. SCE, starting at positive potentials, at different scan rates ranging from 10 to 200 mV s^{-1} at 25 °C. These voltammograms present two large redox pair of peaks A_1/C_1 and A_2/C_2, respectively at the positive and negative potential ranges. Similar voltammograms have been published previously by us [17]. The CVs are stable and their shapes remain unchanged, regardless of the number of cycles. The peak, A_1 ($E = 0.405 \pm 0.005$ V), is located prior to the oxygen evolution on the forward scan, and a small cathodic peak, C_1 ($E = 0.250 \pm 0.005$ V), is observed on the reverse scan. The active species involved are acting as effective transfer mediator for oxygen evolution. These peaks represent the finger print of the solid state Co^{4+}/Co^{3+} redox pair as previously stated for the Co_3O_4 [17]. In this study, also, the redox couple A_1/C_1 is mainly attributed to cobalt species with a small contribution of the iron species and the A_2/C_2 redox couple to the iron species.

In order to study the A_2/C_2 couple, in more detail, the effect of the scan rate on the CV was also investigated. It was found that the peak current intensity increases with increasing the sweep rate up to 150 mV s^{-1}. The ratio between the cathodic $I_{p_{c_2}}$, and the anodic $I_{p_{a_2}}$ peak current intensities, was around unity. A linear relationship between $I_{p_{c_2}}$ (or $I_{p_{a_2}}$) and the square root of scan rate is observed, as the inset of Fig. 2 shows. The linearity and a null intercept are expected for electrochemical processes controlled by mass transfer in solution. The relationship between the peak current I_p and $v^{1/2}$ is given by the Randles–Sevcik equation [34]:

$$I_p = 2.69\ 10^5 S n^{3/2} D^{1/2} c v^{1/2} \quad (4)$$

where I_p is the peak current intensity (A), S the working electrode surface area ($S = 2$ cm^2), n the number of electrons (in this case $n = 2$ see reaction (6) below), D the diffusion coefficient (cm^2 s^{-1}), c the concentration (mol cm^{-3}) and v the scan rate (V s^{-1}).

Although our data show a linear variation of I_p with $v^{1/2}$, a positive intercept is observed indicating that some additional processes other than diffusion in solution could take place, probably diffusion through the solid oxide.

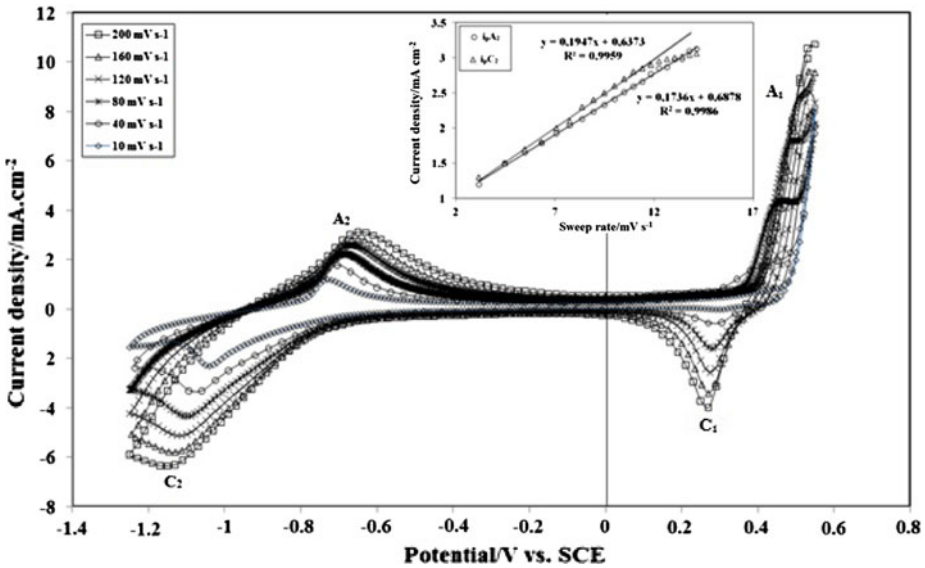

Fig. 2 Cyclic voltammograms for a $CoFe_2O_4$ thin film electrode in an N_2 deoxygenated 1 M KOH solution at different scan rates, starting at 0.500 V vs. SCE scanning towards negative direction. *Inset*: plot of the peak current density vs. the square root of sweep rate for A_2/C_2 redox peaks

For the cathodic peak C_2 the slope of the plot, I_p vs. $v^{1/2}$, is 0.006 C V^{-1} and the voltammetric charge calculated at $v = 0.005$ V s^{-1} is 22×10^{-3} C cm^{-2}. Assuming that this charge is confined in the oxide film, which thickness is 0.3 μm, it gives for the concentration $c = 7.6 \times 10^{-3}$ mol cm^{-3}.

Having in mind that the Randles–Sevcik equation is only applicable for mass transfer in solution, the estimation of the diffusion coefficient D, from the I_p vs. $v^{1/2}$ slope, has been attempted and a value of 1.1×10^{-12} cm^2 s^{-1} was obtained. This value is 100 times lower than 10^{-10} cm^2 s^{-1}, obtained by one of us for the OH^- diffusion coefficient through Co_3O_4 thin films in 1 M KOH, using the same methodology [35].

Figure 3 shows the cathodic current transient, in deoxygenated 1 M KOH, for a potential step from the E_{OC}, −0.120 to −0.800 V. The steady state current is reached at about 10 s. The linearity of the plot I vs. $f(t^{-1/2})$ (Fig. 3, inset), indicates that the reduction is diffusion-controlled. It is obvious that both oxygen and oxide reduction occur, in these conditions, with a limited diffusion of the species through the solid oxide. The extrapolation of the straight line at $I = 0$ intercepts the X-axis at positive values. Calvo and co-workers [36, 37] have reported a similar behaviour for PVC–Fe_3O_4 electrodes in 1 M NaOH saturated with O_2. A model with three-dimensional time-bounded diffusion through the particles has been used to fit the results characterized by the unusual behaviour with a non-zero intercepts [38]. The model allows the determination of the diffusion coefficient of the diffusing particle in the oxide crystals using:

$$C = S/(Dt)^{1/2} \tag{5}$$

where S is the average particle size, D the diffusion coefficient, t the extrapolated time for zero current (Fig. 3) and $C = 2.26$ for cubic crystals [36].

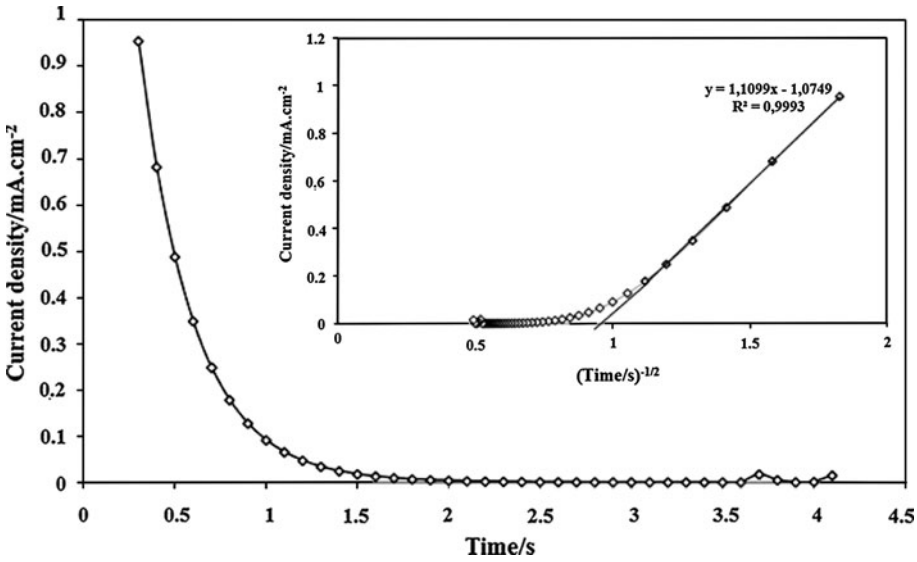

Fig. 3 Current response to a potential step from −0.120 V vs. SCE to −0.800 V vs. SCE for a $CoFe_2O_4$ thin film electrode in an N_2 deoxygenated 1 M KOH solution. *Inset*: plot of I vs. $t^{-0.5}$

The average value, calculated from Eq. 5, for the diffusion coefficient, D, is 1.7×10^{-12} cm^2 s^{-1}. This value compares well with the one estimated from the Randles–Sevcik equation.

3.2.1.2 Pt/iron oxi-hydroxides electrodes To get more insight on the electrochemical processes occurring on $CoFe_2O_4$ oxide electrodes on the cathodic side, electrochemical behaviour of Pt/iron oxi-hydroxides were also investigated. Cyclic voltammograms were performed on Pt/Fe(II)-hydroxide and Pt/Fe(III)-hydroxide at a scan rate of 10 mV s^{-1} in 1 M KOH starting at 0 V vs. SCE in the negative direction. Figure 4a and b show the first and second scans respectively obtained for both hydroxides. For sake of comparison, the CVs for a $CoFe_2O_4$ oxide electrode are also presented.

The first scans are quite similar for all systems, presenting a large pair of peaks, in the negative range of potential. Although the voltammetric profiles for the Fe(III) hydrous electrode present an extra cathodic peak at about −1.0 V vs. SCE, in the subsequent scan, both hydroxide electrodes present a stable I/E profile similar to the $CoFe_2O_4$ electrode.

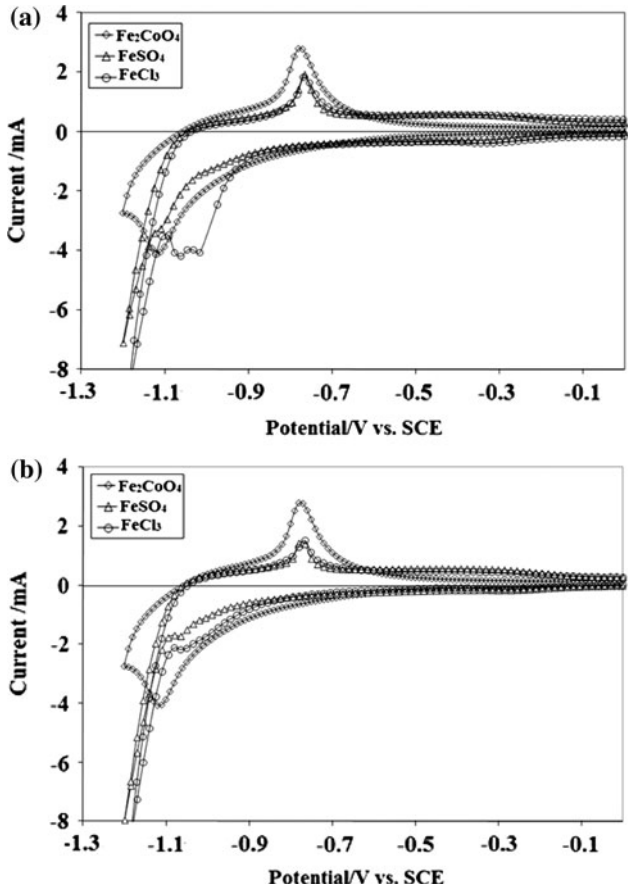

Fig. 4 Cyclic voltammograms for $CoFe_2O_4$ oxide electrode and thin film electrodes of Fe(II)-hydroxide and Fe(III)-hydroxide prepared on Pt from $FeSO_4$ and $FeCl_3$ respectively, in an N_2 deoxygenated 1 M KOH solution. Scan rate of 10 mV s^{-1}, starting at 0 V vs. SCE and scanning towards the negative direction. **a** First cycle and **b** second cycle

Considering that after the first scan, on both iron oxi-hydroxides and $CoFe_2O_4$ electrodes, the peaks appear in the same potential range they can be assigned to the same electrochemical reaction. Vago and Calvo [36] observed peaks, similar to C_2 and A_2, on the Fe_3O_4–PVC composite electrode in 1 M NaOH and assigned them to the reduction of Fe(III) to Fe(II) surface sites followed by its reoxidation, in the reverse potential scan. On the other hand, Cordoba et al. [39] have investigated the precipitation of $FeSO_4$ by NaOH on Pt supports, at different concentrations. They have explained their results, at negative potentials, on the basis of the following redox reactions:

$$Fe_3O_4{\cdot}4H_2O + 2e \rightarrow 3Fe(OH)_2 + 2OH^- \quad -0.900 \text{ V vs. NHE} \tag{6}$$

and

$$\delta\text{-FeOOH} + H_2O + e \rightarrow Fe(OH)_2 + OH^- \quad -0.796 \text{ V vs. NHE} \tag{7}$$

The electrochemical redox transitions on $CoFe_2O_4$ and Fe(II) hydroxide electrodes, involve reaction (6) regardless of the cycle number. On the other hand, the electrochemical redox transition on the Fe(III) hydroxide electrodes involves both reactions (6) and (7) at the first scan, and mainly reaction (6) in the subsequent scan.

Taking into account the assumptions stated above, the diffusion coefficient, previously determined, can be attributed to the diffusion of OH^- through the $CoFe_2O_4$ film. It should be noted that on the reduction process, (reaction 6), two electrons were gained by the oxide film via the substrate and simultaneously two OH^- ions leave the oxide to the electrolyte-facing the film. The diffusion of the OH^- ion through the oxide is the slowest step and so, it acts as the rate-determining step.

3.2.2 Electrochemical impedance spectroscopy

The EIS study of the $CoFe_2O_4$/stainless steel electrodes has been carried out at different constant dc potentials in the potential range from 0 to −1.000 V vs. SCE in 1 M KOH at 25 °C. Prior to the commencement of impedance experiment at a chosen potential, the electrode was first equilibrated at that potential in 1 M KOH for about 300 s. Representative results in both Nyquist and Bode modes are presented in Fig. 5.

Figure 5 shows that at high frequencies, plots, $-Z''$ vs. Z', are almost linear with the slope equal to nearly unity, regardless of the applied dc potential. Some representative

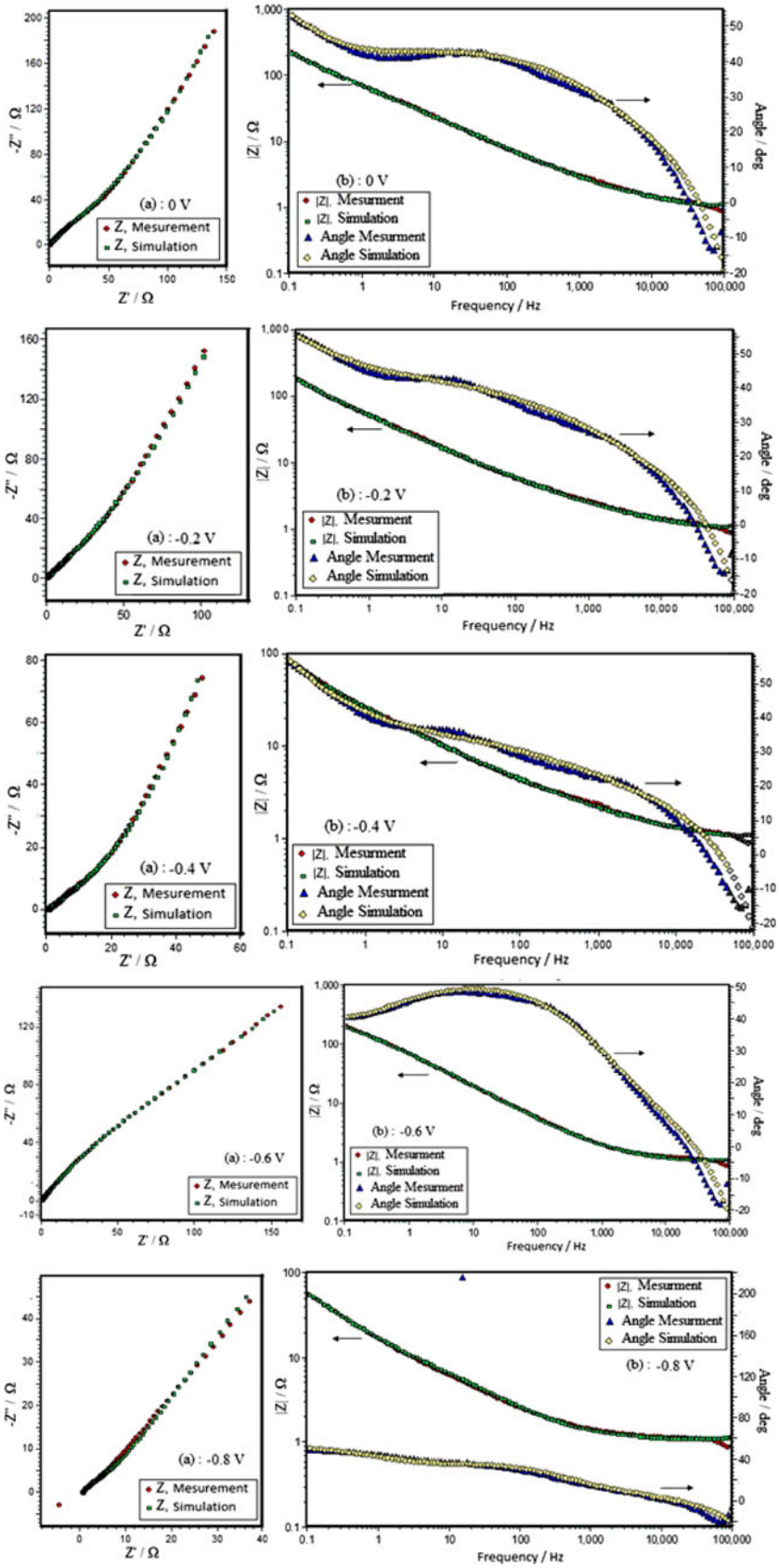

Fig. 5 Complex impedance plots, in Nyquist (**a**) and Bode (**b**) modes (experimental and simulated), for $CoFe_2O_4$ film electrode in an N_2 deoxygenated 1 M KOH solution at different cathodic potentials, 0, −0.2, −0.4, −0.6, −0.8 V vs. SCE

data are also presented in Fig. 6. However, at relatively lower frequencies, the Nyquist plots show a capacitive type behaviour, particularly at the potentials, 0.0, −0.200 and −0.400 V as indicated in Fig. 5 (1a, 2a, and 3a). Similar type of behaviour, at low frequencies, was also observed in the case of Fe–Co_3O_4/1 M KOH interface [21]. These results indicate that at high frequencies (6,329–10 Hz), the diffusion of OH^- ions into the oxide film dominates the impedance results producing a conventional semi-infinite Warburg region, wherein $|\Delta Z''|/|\Delta Z'|$ value is almost unity; the latter value increases from unity with decreasing frequency thereafter and the impedance response appears to be of capacitive nature. Thus, there is a transition between semi-infinite Warburg and finite Warburg regimes at low frequencies, which is a common feature in case of an ion intercalation into inorganic/polymer host matrix [40]. At potentials more negative to −0.400 V, the capacitive curve at low frequencies bends somewhat towards X-axis (i.e. Z'), which may be caused due to surface heterogeneity. The non-observance of a semicircle at high frequencies indicates that the charge transfer resistance is much smaller than the sum of the film and solution resistances [39].

The EIS data were simulated by using a simple equivalent circuit model with the circuit description code, LR_s (R_1Q_1) Q_2. Symbols, R_s and R_1 are the solution resistance

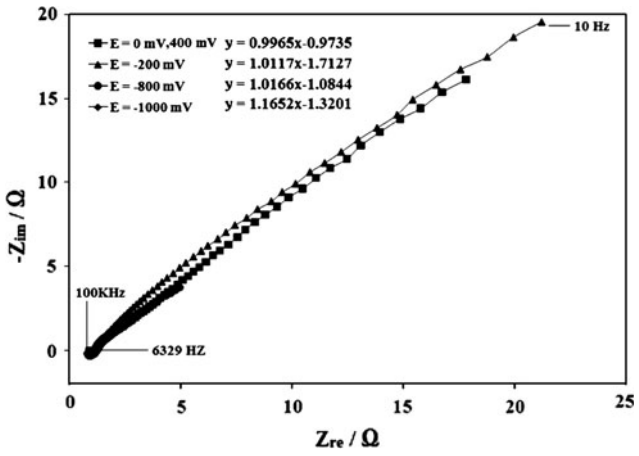

Fig. 6 Nyquist plots ($-Z''$ vs. Z') of $CoFe_2O_4$ film in 1 M KOH solution at different cathodic potentials as indicated on the figure

including the contribution of the oxide matrix and pores resistance, respectively. Q_1 is the CPE and Q_2 is the CPE related to low frequency capacitance. The simulated and experimental data agree quite well as shown in Fig. 5. Estimates of the circuit parameters are listed in Table 1.

Results presented in Table 1 show that n_1 values are close to 0.5, regardless of the applied potentials indicating the contribution of Warburg diffusion at high frequencies. Further, n_2 values are nearly unity, particularly at $E = 0$, −0.200, and −0.400 V indicating, thereby, that they represent the total capacitance, distributed along the pores of nearly the whole film thickness at low frequencies, of the oxide. At potentials more negative to −0.400 V (i.e., at $E = -0.600$ and −0.800 V), the observed significant decrease in n_2 value from unity has been considered to be due to the enhanced surface heterogeneity.

3.2.2.1 Estimation of diffusion coefficient and capacitance value The apparent diffusion coefficient of OH^- ions (D_{ap}) was estimated assuming a transition between semi-infinite and finite Warburg regimes at low frequencies, particularly in the case of Nyquist plots obtained at $E = 0.0$, −0.200 and −0.400 V. The diffusion-controlled regime [$|\Delta Z''|/|\Delta Z'| \approx 1$] is observed from 6,329 to 10 Hz. In this frequency range, the magnitude of the impedance varies linearly with $(\omega)^{-1/2}$ with a slope $= L/CD_{ap}^{1/2}$ [30] (Fig. 7) and is given by Eq. 8.

$$|Z| = L/CD_{ap}^{1/2}\omega^{-1/2} \tag{8}$$

where C, D_{ap} and L are the low frequency redox/limiting capacitance, the diffusion coefficient and the oxide film thickness, respectively. As already reported [30, 31], the C value can be obtained from the low frequency impedance data (charge saturation region: $\omega \ll L^2/D_{ap}$) using Eq. 9, where the locus of each film becomes vertical and that the plot, $-Z''$ vs. $1/\omega$ is linear with slope* $= 1/C$

$$-Z'' = 1/C\omega \tag{9}$$

In the present case, the impedance response is not vertical at very low frequencies, possibly due to surface heterogeneity, however, the plot, $-Z''$ vs. $1/\omega$ is linear as shown in Fig. 8. With the help of Eqs. 8 and 9, the D_a (= slope* × L/Slope)^2 values for OH^- across the oxide film/solution interface was

Table 1 Estimates of the equivalent circuit parameters for the $CoFe_2O_4$ electrodes in 1 M KOH at different cathodic potentials

E/V (vs. SCE)	10^7 L_1/H-cm^2	R_s/Ω-cm^2	R_1/Ω-cm^2	10^3 Q_1/S-s^n/cm^2	n_1	10^3 Q_2/S-s^n/cm^2	n_2
0	8.23	0.89	101.4	5.95	0.5	8.09	0.8
−0.200	8.09	0.88	120.1	10.66	0.5	10.92	0.80
−0.400	8.43	0.85	500.2	20.08	0.4	36.51	1
−0.600	7.66	0.98	140.4	6.78	0.6	1.14	0.6
−0.800	7.21	1.04	4.63	16.56	0.6	24.44	0.6

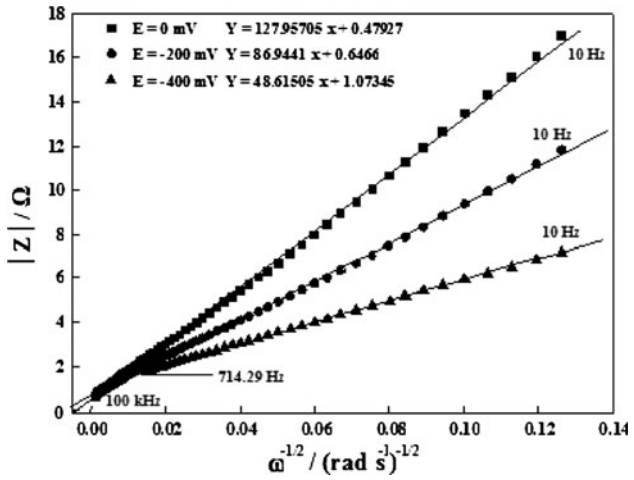

Fig. 7 Plots of $|Z|$ vs. $\omega^{-1/2}$ for semi-infinite diffusion data for the $CoFe_2O_4$ film

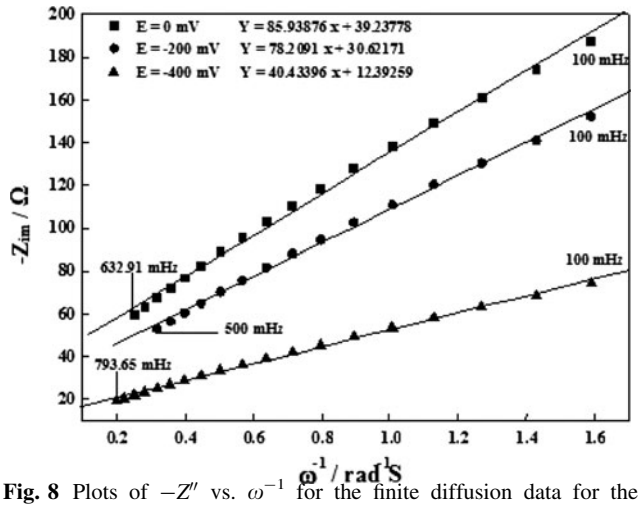

Fig. 8 Plots of $-Z''$ vs. ω^{-1} for the finite diffusion data for the $CoFe_2O_4$ film

estimated at the dc potentials of 0.0, −0.200, and −0.400 V and the obtained values, were 5.1, 7.2 and 6.2×10^{-10} cm^2 s^{-1}, respectively. These values are approximately 100 times higher than those determined, in this study, by CV and chronoamperometry. The D_{ap} value of an ion into a thin porous matrix, determined by the three different techniques, may be different. As an example, Paulse and Pickup [41] obtained D_{ap} values of 3.5×10^{-8} and 1.1×10^{-6} cm^2 s^{-1} by chronoamperometry using the migration and diffusion models, respectively. Monk and Farooq [42] obtained a D_{ap} value of 2.3×10^{-8} cm^2 s^{-1} for diffusion of OH^- ions into the electrodeposited CoO–OH film by CV at room temperature.

Values of C determined from the slope of Fig. 8 are found to be 1.16, 1.28 and 2.47×10^{-2} F cm^{-2} at $E = 0$, −0.200 and −0.400 V, respectively. These values differ only marginally from those corresponding, Q_2, values estimated from the equivalent circuit.

4 Conclusion

Spinel type $CoFe_2O_4$ thin films were prepared on stainless steel by thermal decomposition of nitrates. The value of the unit cell parameter, a_0, of $CoFe_2O_4$ oxide coatings was found to be 8.385 Å using X-ray analysis. The $CoFe_2O_4$/electrolyte interface has been investigated in 1 M KOH, in the potential region of oxygen reduction, by cyclic voltammetry, chronoamperometry and electrochemical impedance techniques. These studies allowed identifying the redox reactions occurring at the oxide surface in the negative potential range. In addition, it has been concluded that the processes are diffusion-controlled and the diffusion of the hydroxide ion, through the oxide, acts as the rate-determining step. The results are compared with the colloidal electrode prepared by alkaline precipitation of Fe(II) or Fe(III) hydrous oxi-hydroxides on platinum support.

The diffusion coefficient of OH^- ions across the oxide film/solution interface was estimated by cyclic voltammetry and chronoamperometry and the obtained values are similar, 1.1×10^{-12} and 1.7×10^{-12} cm^2 s^{-1}, respectively. The diffusion coefficients of OH^- across the oxide film/solution interface, estimated by EIS at 0.0, −0.2, and −0.4 V, were 5.1, 7.2 and 6.2×10^{-10} cm^2 s^{-1}, respectively.

Acknowledgments The authors gratefully acknowledge the support of this study by the Pôle de Compétences Electrochimie-Corrosion et Chimie Analytique (PECCA), Ministère de l'Education Nationale, de l'Enseignement Supérieur, de la Formation des Cadres et de la Recherche Scientifique.

References

1. Mohan H, Saikh IA, Kulkaarni RG (1992) Solid State Commun 82:907
2. Alcantara R, Jaraba M, Lavela P et al (2002) In: Electrochemical society meeting, Salt Lake City, p 131
3. Lavela P, Tirado JL (2007) J Power Sources 172:379
4. Ayn Li, Qin Q (2005) J Power Sources 142:292
5. Singh RN, Singh NK, Singh JP (2002) Electrochim Acta 47:3873
6. Singh RN, Lal B, Malviya M (2004) Electrochim Acta 49:4605
7. Sartal SD, Ganesan V, Lokhande CD (2005) Phys Status Solidi 202:85
8. Sartal SD, Lokhande CD (2002) Ceram Int 8:467
9. Kishi T, Takahashi S, Nagai T (1986) Surf Coat Technol 27:351
10. Cartaxo MAM, Ferreira TAS, Nunes MR et al (2007) Solid State Sci 9:744
11. Okazaki Y, Lixin M, Ohya Y et al (2007) J Mater Process Technol 181:66
12. Chunye Z, Xiangqian S, Jianxin Z et al (2008) Rare Met Mater Eng 37:108
13. Bellad SS, Bhosale CH (1998) Thin Solid Films 322:93
14. Zhang G, Xu W, Li Z et al (2009) J Magn Magn Mater 321:1424
15. Jiao Z, Geng X, Wu M et al (2008) Colloids Surf A 313–314:31
16. Godinho MI, Catarino MA, da Silva Pereira MI et al (2002) Electrochim Acta 47:4307
17. Laouini E, Berghoute Y, Douch J et al (2009) J Appl Electrochem 39:2469

18. Singh RN, Singh JP, Lal B et al (2006) Electrochim Acta 51:5515
19. Laouini E, Hamdani M, Pereira MIS et al (2008) Int J Hydrog Energy 33:4936
20. Laouini E, Hamdani M, Pereira MIS et al (2008) J Appl Electrochem 38:1485
21. Laouini E, Hamdani M, Pereira MIS et al (2009) Int J Electrochem Sci 4:1074
22. Silva GC, Fugiwara CS, Tremiliosi Filho G et al (2002) Electrochim Acta 47:1875
23. Wu G, Li N, Zhou DR et al (2004) J Solid State Chem 177:3682
24. Palmas S, Ferrara F, Mascia M et al (2009) Int J Hydrog Energy 34:1647
25. Singh RN, Mishra D, Anindita et al (2007) Electrochem Commun 9:1369
26. Palmas S, Ferrara F, Vacca A et al (2007) Electrochim Acta 53:400
27. Lal B, Singh NK, Samuel S et al (1999) J New Mater Electrochem Syst 2:59
28. Singh JP, Singh RN (2000) J New Mater Electrochem Syst 3:137
29. Ho C, Raistrick ID, Huggins RA (1987) J Electrochem Soc 134:142
30. Penner RM, Martin CR (1989) J Phys Chem 93:984
31. Naoi K, Ueyama K, Osaka K et al (1990) J Electrochem Soc 137:494
32. Fradette N, Marsan B (1998) J Electrochem Soc 145:2320
33. Wang J, Deng T, Lin Y et al (2008) J Alloy Compd 450:532
34. Bard AJ, Faulkner LR (1980) Electrochemical methods, fundamentals and applications. Wiley, New York
35. Hamdani M, Koenig JF, Chartier P (1988) J Appl Electrochem 18:568
36. Vago ER, Calvo EJ (1992) J Electroanal Chem 339:41
37. Calvo J, Drennan J, Kilner JA, Yeager EB (eds) (1984) The chemistry and physics of electrocatalysis. Electrochemical Society, Pennington, p 489
38. Van Buren FR, Broers GHJ, Bouman AJ et al (1978) J Electroanal Chem 87:353
39. Cordoba SI, Carbonio RM, Lopez Teijelo M et al (1986) Electrochim Acta 31:1321
40. Singh RN, Malviya M, Anindita, Sinha ASK, Chartier P (2007) Electrochim Acta 52:4264 and references therein
41. Paulse CD, Pickup PG (1988) J Phys Chem 92:7002
42. Monk PMS, Farooq N (1995) J Mater Sci Mater Electron 6:389